JACS
JOURNAL OF THE AMERICAN CHEMICAL SOCIETY

Article

pubs.acs.org/JACS

# Direct Formation of Large-Area 2D Nanosheets from Fluorescent Semiconducting Homopolymer with Orthorhombic Crystalline Orientation

Sanghee Yang, Suyong Shin, Inho Choi, Jaeho Lee, and Tae-Lim Choi*

Department of Chemistry, Seoul National University, Seoul 151-747, Korea

Supporting Information

**ABSTRACT:** Semiconducting polymers have been widely investigated due to their intriguing optoelectronic properties and their high crystallinity that provides a strong driving force for self-assembly. Although there are various reports of successful self-assembly of nanostructures using semiconducting polymers, direct *in situ* self-assembly of these polymers into two-dimensional (2D) nanostructures has proven difficult, despite their importance for optoelectronics applications. Here, we report the synthesis of a simple conjugated homopolymer by living cyclopolymerization of a 1,6-heptadiyne (having a fluorene moiety) and its efficient *in situ* formation of large-area 2D fluorescent semiconducting nanostructures. Using high-resolution imaging tools such as atomic force microscopy and transmission electron microscopy, we observed the solvent-dependent self-assembly behaviors of this homopolymer; the identical starting polymer formed 2D nanosheets with different shapes, such as rectangle, raft, and leaf, when dissolved in different solvents. Furthermore, super-resolution optical microscopy enabled the real-time imaging of the fluorescent 2D nanosheets, revealing their stable and uniform shapes, fluorescence, and solution dynamics. Notably, we propose an orthorhombic crystalline packing model to explain the direct formation of 2D nanostructures based on various diffraction patterns, providing important insight for their shape modulation during the self-assembly.

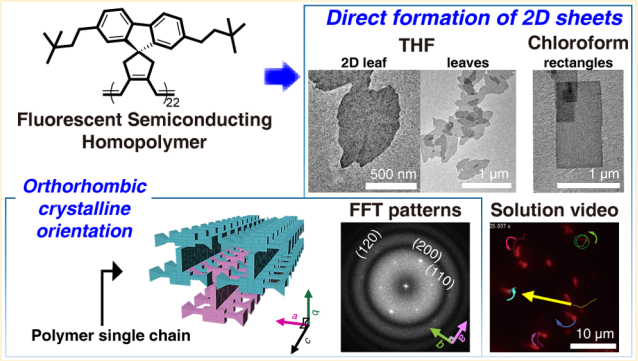


## INTRODUCTION

Self-assembly of amphiphilic block copolymers (BCPs) has become a general strategy for producing diverse morphologies in solution,[1] ranging from simple spherical micelles[2] to higher-order nanostructures.[3] Among them, well-ordered semiconducting materials prepared from various conjugated polymers[4] have been intensively investigated due to their potential for increasing optoelectronic performance in many devices, such as light-emitting diodes,[5] transistors,[6] and photovoltaics.[7] However, most of the self-assembly processes using soft materials rely on the principles of phase separation under specific conditions; this approach thus requires sophisticated chemical design of amphiphilic BCPs, or BCPs having blocks with significant solubility differences. Further, post-treatments such as dialysis,[3d] addition of reagent or selective solvents,[8] temperature modulation,[9] and aging[10] are often necessary to induce self-assembly. Recently, our group developed an *in situ* nanoparticlization of conjugated polymers (INCP) process by introducing strong $\pi-\pi$ interactions on the second block to promote kinetically trapped self-assembly during living polymerization. For example, during the synthesis of BCPs having a soluble first block and insoluble polyacetylene (PA) or polythiophene (PT) on the second block, highly stable nanoparticles of spheres, one-dimensional nanocaterpillars, stars, and networks formed spontaneously.[11] In other words, the most significant advantage of INCP is that it enables the direct formation of various semiconducting nanomaterials without post-treatment, allowing for simple and mass production of such materials. Nevertheless, despite the recent advances in INCP and other unique approaches such as polymerization-induced self-assembly (PISA),[12] the preparation of two-dimensional (2D) structures via *in situ* self-assembly remains an unsolved problem.

Among the various multidimensional nanostructures, 2D materials, especially graphene, have received the most attention due to their intriguing electronic performances with broad applications such as sensors and transistors.[13] For decades, there have been efforts to prepare new 2D organic materials, but introducing an anisotropic orientation remains challenging. Therefore, flat molecules were commonly required to afford the periodic anisotropic bonding via covalent and coordination polymerization.[14] However, only a few examples of the self-assembly of 2D nanostructures from polymers have been reported. For example, 2D nanostructures were prepared from conjugated graft copolymers via temperature modulation[5a] and from poly(3-hexylthiophene)-*block*-poly(ethylene glycol) (P3HT-*b*-PEG) by the air–liquid interfacial method.[15]

**Received:** December 3, 2016
**Published:** February 16, 2017

ACS Publications © 2017 American Chemical Society



DOI: 10.1021/jacs.6b12378
J. Am. Chem. Soc. 2017, 139, 3082–3088

Recently, uniform 2D platelet micelles were prepared by blending crystalline homopolymers and BCPs via a crystalline-driven self-assembly (CDSA) process in selective solvents.[16a,b] In addition, other lamellar morphologies were obtained from a blend of BCP and nonconjugated homopolymers acting as a structural trigger.[16c,d] However, the synthesis of 2D nanostructures from simple homopolymers alone is very rare and requires harsh temperature modulation.[8b] Therefore, direct and post-treatment-free synthesis of 2D nanostructures from *in situ* nanoparticlization of simple homopolymers would greatly simplify the production process of functional 2D nanomaterials.

Here, we demonstrate a new *in situ* formation of various large-area 2D nanostructures resembling leaves, rectangles, and rafts by the living cyclopolymerization of a 1,6-heptadiyne monomer containing a fluorene moiety. Based on high-resolution transmission electron microscopy (HR-TEM) and X-ray diffraction (XRD) analysis, we suggest that orthorhombic crystalline packing of the resulting poly(cyclopentenylene-vinylene) (PCPV) is the basis of 2D sheet formation. To fully investigate the structural properties of the 2D structures, we use atomic force microscopy (AFM), TEM, and super-resolution optical microscopy to monitor their real-time dynamics in solution.

## RESULTS AND DISCUSSION

Based on our early investigations on the living cyclopolymerization of 1,6-heptadiynes that produced five-membered PA exclusively,[17] we envisioned that this reaction could lead to an INCP process even with homopolymer architectures. Therefore, we designed new 1,6-heptadiyne monomers (**M1** and **M2**) containing a fluorene moiety, hoping that the additional $\pi-\pi$ interactions between fluorenes would maximize intermolecular interaction of packing, thereby forming new nanostructures.[18] Using the third-generation Grubbs catalyst (**G3**), **M1** and **M2** were polymerized at a monomer-to-initiator ratio ([M]/[I]) of 22 in tetrahydrofuran (THF) at 0 °C (Scheme 1 and Table S1). The reaction was then quenched by

**Scheme 1. Scheme of Living Cyclopolymerization of M1−M3**

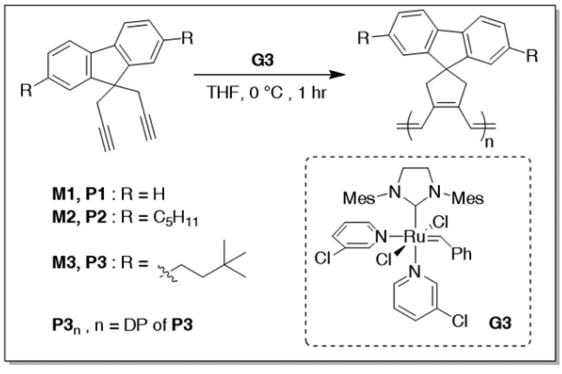


addition of excess ethyl vinyl ether and precipitated in methanol at room temperature to give a dark solid. As expected, the resulting polymers **P1** and **P2** immediately underwent a successful INCP process in solution (supported by dynamic light scattering (DLS) analysis showing a hydrodynamic diameter ($D_h$) of 858 nm for **P1** and 279 nm for **P2** in THF solution, Figure S2). However, unfortunately AFM and TEM imaging only revealed irregular nanoaggregates from the THF solution of **P1** and **P2** (Figure S3). Apparently, these homopolymers induced overly strong intermolecular $\pi-\pi$ interactions between the fluorenes as indicated by film X-ray diffraction (FXRD) and their low solubility, thereby forming irregular nanoparticles (Figure S4).

To obtain well-defined nanostructures, we introduced bulky neohexyl groups on the fluorene (**M3**) to weaken the $\pi-\pi$ interactions. As expected, the resulting **P3** showed improved solubility in THF, so that living cyclopolymerization with various [M]/[I] ratios up to 40 could be employed to prepare **P3** having narrow polydispersity index (PDI) and a higher degree of polymerization (DP) than **P1** and **P2** (Figures 1a and S5 and Table S1). Furthermore, this new **P3** seemed to exhibit some different electronic property, as compared to **P1** and **P2**. UV−vis analysis indicated that, although **P1**−**P3** (DP = 22) all showed common absorption at 300 nm corresponding to the fluorenes, the absorption for the conjugated backbone of **P3** from 400 to 600 nm was stronger in intensity and more red-shifted compared to **P1** and **P2** (Figure 1b). The $\lambda_{max}$ of **P3** in THF was at 549 nm, higher than **P1** and **P2** and poly(dihexyldipropargylmalonate) (PDHDPM), a conventional PCPV.[19] Moreover, the 0−0 vibronic band of **P3** appeared at 590 nm and it was 13 nm longer than that of PDHDPM (Figure 1b), implying that **P3** showed more extended and stiffer polymer chains than any other PCPVs. From $^1$H NMR and IR analyses, all the produced olefins on the conjugated backbone of **P3** were *E*-isomers, and this also agreed with its extended conformation (Figure S1).

Initially, we expected the nanostructures from the much more soluble **P3** to show the smallest $D_h$ in THF among the homopolymers **P1**−**P3** at the same DP of 22. However, the $D_h$ of $\mathbf{P3}_{22}$ at 1 mg/mL was 1.6 $\mu$m, much larger than those of **P1** and **P2** (Figures 1c and S2). An even bigger surprise was that when visualized by AFM and TEM at 1 mg/mL, this unexpectedly large microsized supramolecular structure spontaneously formed well-defined 2D sheets resembling leaves via an INCP process (Figure 2). Detailed investigation showed that the height of a single layer 2D leaf increased from 8 to 11 nm with an increase of DP from 15 to 22 (Figure S10). Interestingly, the double layer 2D sheets showed twice the height value of 22 nm (The height profiles shown in the inset of Figure 2c). To support the *in situ* nanoparticlization, we took an *in situ* sample during polymerization of $\mathbf{P3}_{15}$ (at DP = 15) without any quenching and purification steps and the same 2D leaves were obtained by TEM (Figure 2b). However, one would notice that there were some small messy aggregates on the background presumably due to the incomplete self-assembly. Furthermore, we conducted cryogenic TEM imaging from the THF solution of the purified $\mathbf{P3}_{22}$ to prove that the nanoparticlization did occurred in solution, not by drying process and indeed the same 2D leaves were observed confirming their same intrinsic morphology in solution and the dry state (Figure S8).

When the same purified $\mathbf{P3}_{22}$ (DP = 22) after workup was dissolved in chloroform and dichloromethane (DCM) solutions, $D_h$ > 1.5 $\mu$m was also detected (Figure 1c). Interestingly, UV−vis analysis of $\mathbf{P3}_{22}$ in chloroform showed a more red-shifted spectrum with $\lambda_{max}$ = 560 nm and a stronger 0−0 vibronic band at 602 nm, higher than those in THF or DCM solution at least by 11 nm (Figure 1d). This observation implied the most extended and stiffest conformation of $\mathbf{P3}_{22}$ in chloroform. Surprisingly, AFM and TEM imaging from these solutions revealed very different 2D nanostructures: microsized


DOI: 10.1021/jacs.6b12378
J. Am. Chem. Soc. 2017, 139, 3082−3088

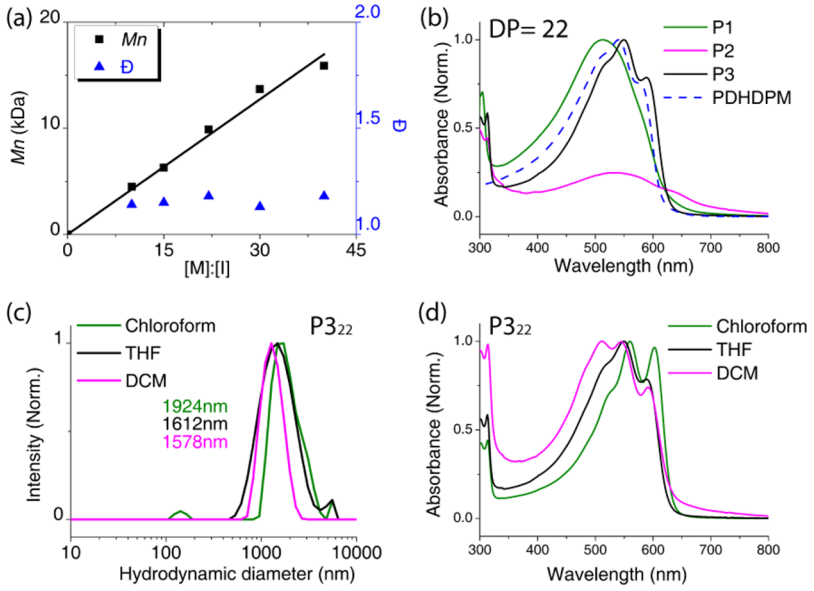


**Figure 1.** (a) Plot of the molecular weight ($M_n$) versus the [M]:[I] ratio and polydispersity index. (b) UV−vis spectra of **P1**−**P3** (solid line), and PDHDPM (dashed line) in THF (0.1 mg/mL). (c) Size measurements of $\mathbf{P3}_{22}$ by DLS analysis in three solvents (1 mg/mL). (d) UV−vis spectra of $\mathbf{P3}_{22}$ in three different solvents (0.1 mg/mL).

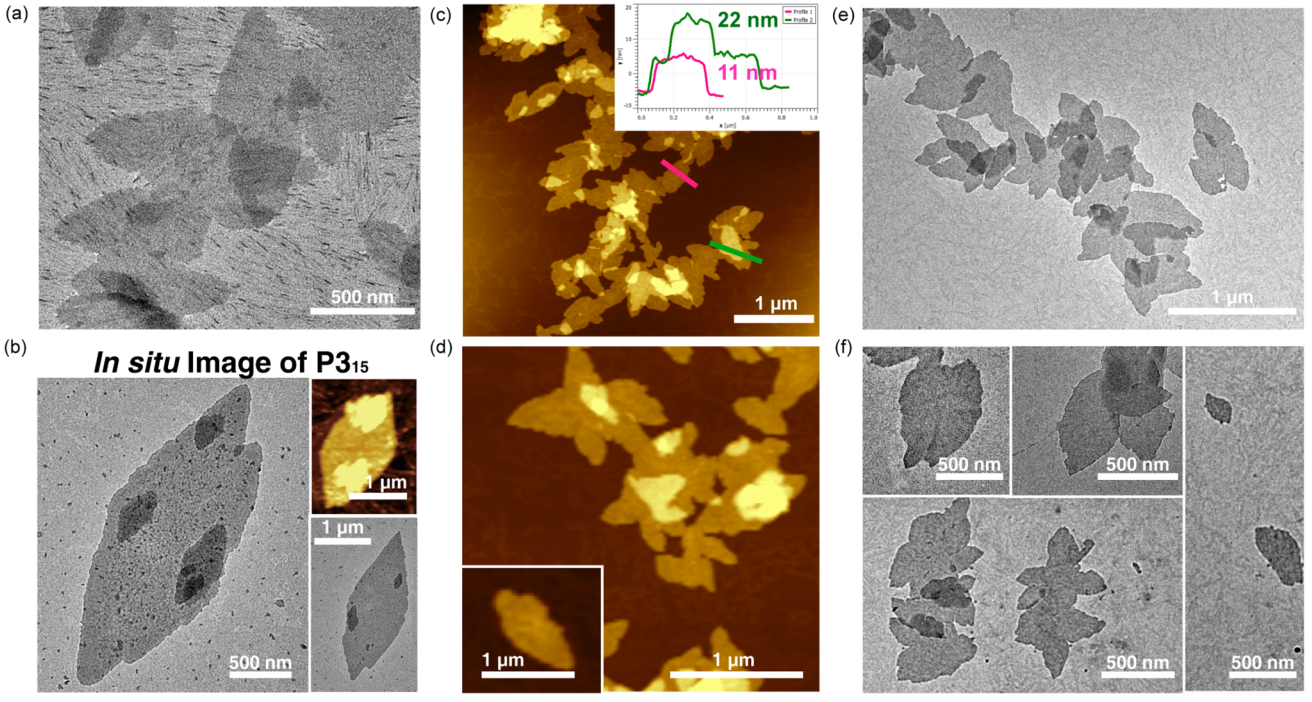


**Figure 2.** AFM and TEM images of (a) $\mathbf{P3}_{15}$ (DP = 15) in THF after precipitation and (b) *in situ* sample during the polymerization in THF: single layer of 2D leaf structures were formed via an INCP process (1 mg/mL). (c−f) AFM and TEM images of $\mathbf{P3}_{22}$ (DP = 22) in THF after precipitation (1 mg/mL). The inset of (c) shows height profiles of the single layer of 2D leaf (11 nm) and double layer of 2D leaves (22 nm).

2D rectangles with almost 90° angles were formed in chloroform (Figure 3a,b), while somewhat irregular 2D sheets resembling rafts were observed from the identical $\mathbf{P3}_{22}$ in DCM (Figure 3c,d). To investigate concentration dependency of the 2D nanosheet formation, DLS measurement, UV−vis analysis, and TEM imaging under very dilute concentration confirmed that these nanostructures were retained even at 0.001 mg/mL (Figures S6 and S7), although 1 mg/mL solution of $\mathbf{P3}_{22}$ seemed to form the most uniform 2D sheets in all three solvents. Finally, cryogenic TEM imaging at low concentrations of 0.01 and 0.03 mg/mL also confirmed the same morphologies in both solution states (Figure S8). Interestingly, despite the different morphologies (leaf, rectangle, and raft) in the three solutions (Figures 2 and 3), the average heights of the single 2D sheet measured by AFM were almost identical (Figure 3e). Moreover, we measured the average heights of the single 2D sheet of **P3** with various DPs in the three solvents and found that their average heights also increased from 5 to 20 nm, proportional to the DP (from 10 to 40) (see Figures 3e, S9, and S10 for the detailed shapes of nanostructures and height



DOI: 10.1021/jacs.6b12378
J. Am. Chem. Soc. 2017, 139, 3082−3088

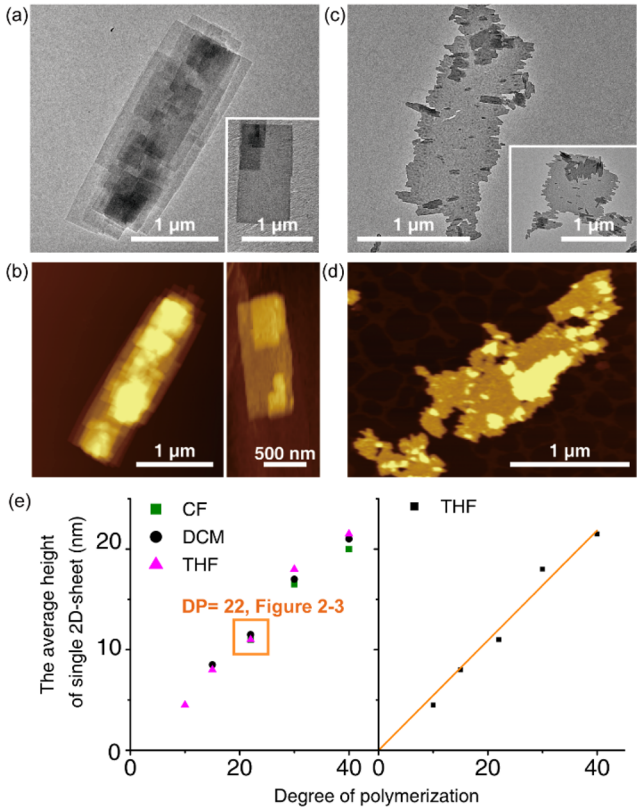


**Figure 3.** AFM and TEM images of (a,b) 2D rectangles from $\mathbf{P3}_{22}$ in chloroform and (c,d) 2D rafts from the identical $\mathbf{P3}_{22}$ in DCM (1 mg/mL). (e) Height information from the various 2D nanosheets in three solutions and linear fitting of average height versus DP of **P3** in THF.

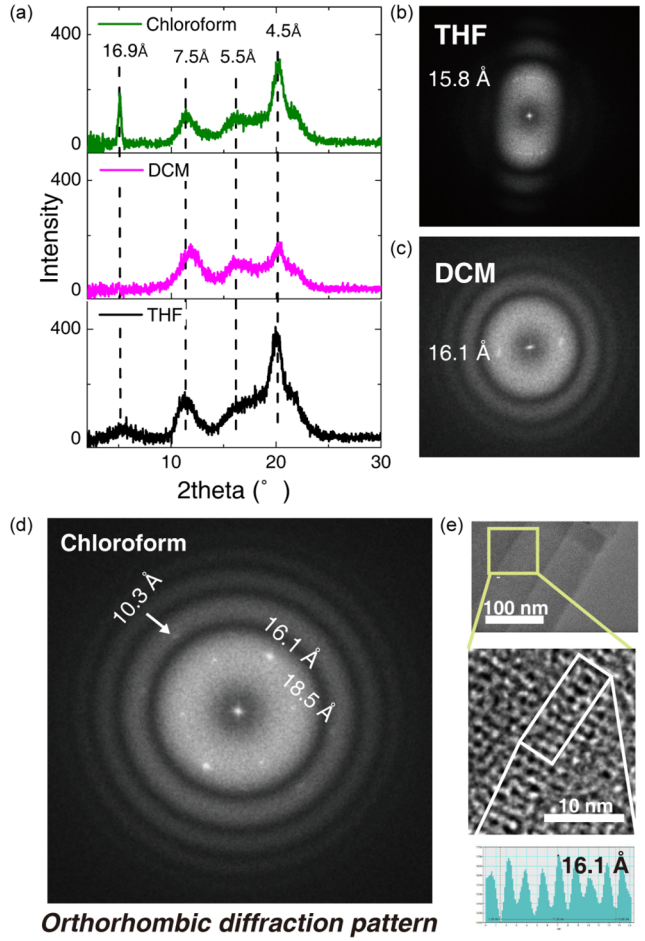


**Figure 4.** (a) Film X-ray diffraction data of the film prepared from the three different solutions of $\mathbf{P3}_{22}$ (10 mg/mL). (b–d) Fast Fourier transform of high-magnification images from three different 2D sheets: (b) 2D leaves in THF, (c) 2D rafts in DCM, and (d) 2D rectangles in chloroform, showing the most ordered diffraction patterns. (e) Parallel stacking of 2D rectangles and uniform crystalline arrays. From an additional cross-sectional histogram, *d*-spacing of 16.1 Å was also calculated from the difference in electron density.

profiles for all entries). A plot of the average height vs the DP of **P3** provided an excellent linear fit and the same trend held for all three nanostructures. In summary, we synthesized semiconducting $\mathbf{P3}_n$ with band gap of 1.96 eV (Figures S16 and S17) that spontaneously produced large-area 2D nanosheets without any tedious post-treatment, and the shapes and heights of 2D sheets were determined by the solvents and the DP.

In order to understand how these unique 2D sheets formed, detailed information on the crystallinity of those 2D sheets were collected from FXRD of the three $\mathbf{P3}_{22}$ solutions. Contrary to our expectations, the *d*-spacing between 3 and 4 Å corresponding to the conventional $\pi-\pi$ interaction of conjugated moieties was completely absent (Figure 4a). Instead, $\mathbf{P3}_{22}$ exhibited common *d*-spacings of 4.5, 5.5, and 7.5 Å in the three samples. This absence of $\pi-\pi$ interactions was in sharp contrast to the well-known examples of conjugated polymers such as poly(3-alkylthiophenes)[20a,b] and poly(*p*-phenylene ethynylene),[20c] which folded into a lamellar packing as a result of the strong $\pi-\pi$ interactions between their conjugated backbones. This unexpected FXRD result led us to suspect that the main driving force for the direct 2D sheet formation of $\mathbf{P3}_{22}$ was not $\pi-\pi$ interactions by the fluorene side chains or the PA main chains. Notably, FXRD of the sample from the chloroform solution alone showed a very sharp peak at 16.9 Å, whereas that peak was much weaker and broader in the sample from THF and disappeared in the sample from DCM solution (Figure 4a).

More insight on the crystallinity was obtained from the electron diffraction pattern by fast Fourier transform (FFT) analysis of HR-TEM micrograms and selected area electron diffraction (SAED) analysis. The diffraction pattern gave direct information on the crystalline orientation at the focused nanostructures of interest (Figures 4b–d, S12, and S13). As a result, all 2D nanosheets had the main *d*-spacing as a diffraction spot near 16 Å (THF, 15.8 Å; DCM, 16.1 Å; and chloroform, 16.1 Å). Particularly, a line at 15.8 Å and not a point was observed for the THF sample, and this explained the round shape of the 2D leaves having less directionality than the other samples (Figures 4b, S12, and S13). On the other hand, 2D rectangles from the chloroform sample showed a highly ordered diffraction pattern corresponding to the orthorhombic crystalline lattice with three main *d*-spacing values of 10.3, 16.1, and 18.5 Å (Figure 4d). Moreover, the direction of the main *d*-spacing at 16.1 Å matched the parallel edge line of the stacked 2D rectangles. Furthermore, we could observe the same crystalline lattice and *d*-spacing of 16.1 Å in electron density profiles from highly magnified images (Figure 4e).

Before solving the diffraction pattern, we inspected the structure of individual $\mathbf{P3}_{22}$ chains in more detail. First, we obtained single-crystal XRD (SC-XRD) of **M3** revealing that the fluorene side chains should be orthogonal to the PA conjugated backbone because of the $sp^3$ hybridized carbon


DOI: 10.1021/jacs.6b12378
J. Am. Chem. Soc. 2017, 139, 3082–3088

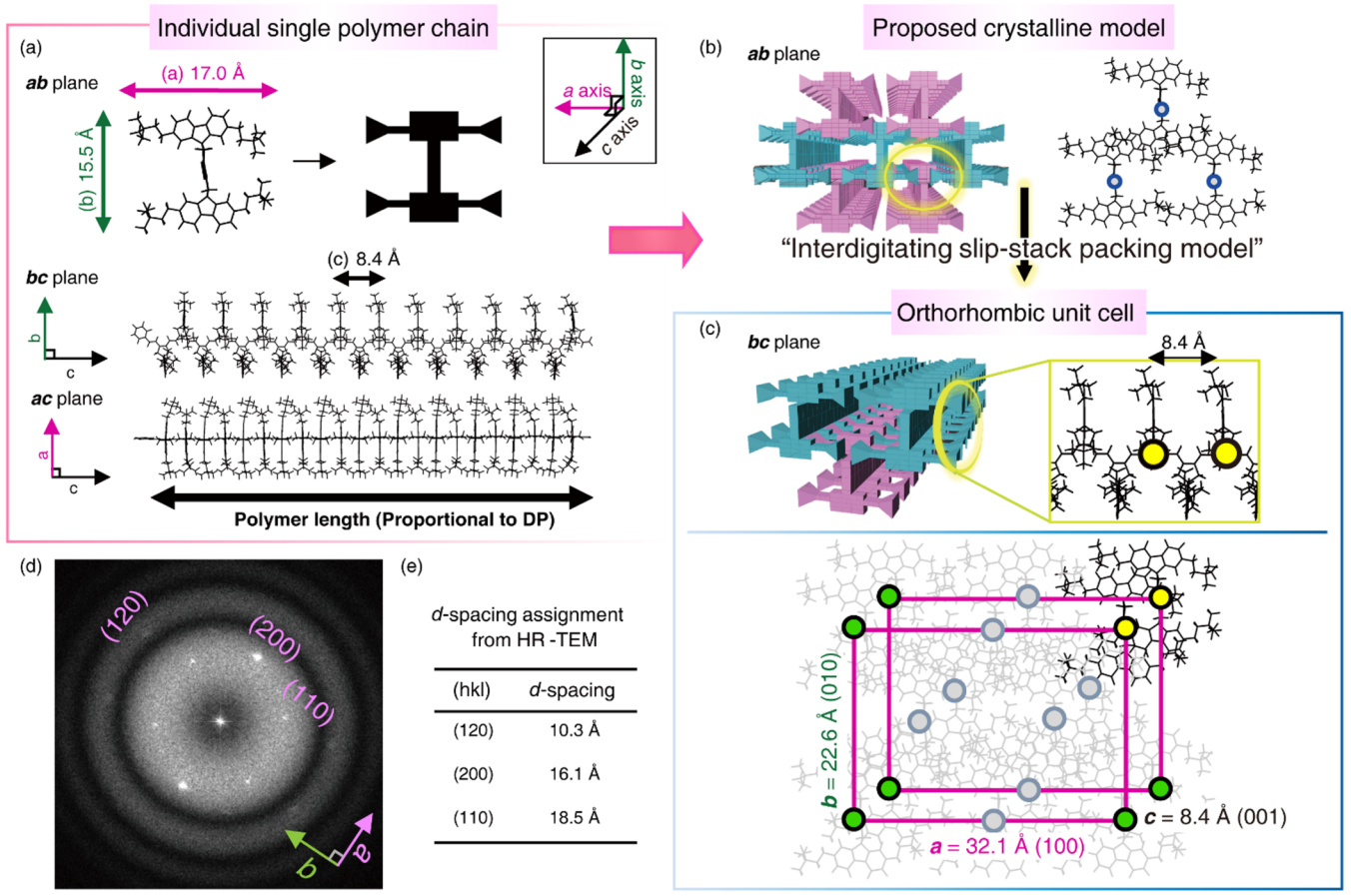


**Figure 5.** (a) Proposed structure of the individual $\mathbf{P3}_{22}$ single chain with estimated distance for three axes. (b,c) 3D schematic illustration of 2D sheet based on the interdigitating slip-stack packing model and 2D arrangement of **P3** based on the proposed structure from (a) with *ab* and *bc* planes. Based on the proposed model, an orthorhombic unit cell with the following calculated lattice parameters was proposed. (d,e) Interpretations of all *d*-spacings from diffraction patterns of 2D rectangles. Three inset values indicate the (*hkl*) planes according to the diffraction spots and their *d*-spacings.

geometry (Figure S15). Based on the lattice parameters of SC-XRD of **M3**, the *a* axis and *b* axis of the **P3** single chain were estimated at 17.0 and 15.5 Å respectively, and the *c* axis corresponded to the length of the PA backbone (Figure 5a, see *ab*, *bc*, and *ac* planes). Since the all-*trans* configuration of $\mathbf{P3}_{22}$ put the adjacent fluorenes on opposite sides, the next neighboring fluorene (*n*+2) would be separated by approximately 8.4 Å (Figure 5a, view for *bc* plane). The absence of $\pi-\pi$ interactions was explained from these $\mathbf{P3}_{22}$ single-chain structures because the intermolecular distance between PA backbones was too far away due to the large orthogonal fluorene side chains (Figure 5a, view for *ac* plane). Furthermore, face-on stacking between the fluorene rings was also disrupted by the bulky side chains (neohexyl groups). Therefore, $\mathbf{P3}_{22}$ in chloroform formed crystalline 2D rectangles packed in a unique orthorhombic lattice without the conventional $\pi-\pi$ interactions of the conjugated polymers.

In order to explain the strong driving force for the spontaneous formation of 2D nanosheets in solution, we proposed a new unique interdigitating slip-stack packing model with a 2D orientation of the **P3** (Figure 5b,c). The first rationale in this model was that an insertion of neohexyl groups into the fluorene–fluorene gap would be energetically more favored over face-on stacking between the aromatic fluorenes having bulky neohexyl groups on top of each other. Then, two neohexyl groups from two separate **P3** chains would intercalate inbetween two fluorene rings on the third **P3** chain putting those neohexyl groups on the fluorene ring (Figure 5b). Indeed, the distance between the neighboring fluorenes on the **P3** chain (~8.4 Å) was large enough for the intercalation of a neohexyl group (radius of 5.2 Å). Additional stabilization via CH–$\pi$ interactions between large aromatic fluorene and neohexyl groups would strengthen the interdigitated 2D arrangement.[21] The 3D schematic illustration in Figure 5b shows the repeated intercalation between the fluorenes and the neohexyl groups based on the interdigitating slip-stack packing model. Finally, we propose the whole 2D arrangement of **P3** in Figure 5c, showing a crystallographic model of a cross-sectional *ab* plane in which the lattice points of the orthorhombic cell were positioned on the five-membered rings of the PA backbones (Figure 5b,c, see *ab* and *bc* planes). As a result, *a*, *b*, and *c* lattice parameters were estimated as *a* = 32.1 Å, *b* = 22.6 Å, and *c* = 8.4 Å (Figure 5c). This orthorhombic unit cell fully explained all of the diffraction patterns from HR-TEM and FXRD in Figures 5d and 4a, respectively. The major diffraction showing 16.1 Å as the *d*-spacing from HR-TEM of three different 2D sheets corresponded to the (200) plane, and this roughly matched the 16.9 Å peak from FXRD of the 2D rectangles in chloroform (Figure 4a). In addition, higher-order diffraction patterns from the HR-TEM of 2D rectangles were assigned: 18.5 Å as *d*-spacing of the (110) plane and 10.3 Å as *d*-spacing of the (120) plane (Figure 5e). Furthermore, the


DOI: 10.1021/jacs.6b12378
J. Am. Chem. Soc. 2017, 139, 3082–3088

crystallinity bands between 4 and 8 Å from the FXRD analysis in Figure 4a corresponded to 7.6 Å from the (111) plane, 5.5 Å from the (131) plane, and 4.2 Å from the (002) plane (see Table S2 for details). As another conclusion of this proposed model, we suggest that the length of the single polymer chain corresponds to the average height of 2D nanosheets. This explained why the height of the single 2D sheet was directly proportional to the DP of **P3** and the heights of various 2D nanosheets obtained from three different solutions of the identical **P3** were very similar to one another despite the different morphologies (Figure 3e). In short, the HR-TEM, FXRD, UV−vis, and AFM analyses strongly supported the *in situ* formation of the 2D nanosheets based on this unique orthorhombic crystal lattice. Although we are not certain at this point as to why the choice of the solvent resulted in different morphologies as shown in Figures 2 and 3, it seems clear that $\mathbf{P3}_{22}$ in chloroform—showing the most extended single-chain conformation—could form the most crystalline domain and the most well-ordered 2D rectangular nanostructures among the three cases (Figures 1d and 4a,d,e). In other words, defects on the crystallinity from the DCM and THF solution might lead to the formation of the less regular 2D raft or even round shapes of 2D leaves. Furthermore, this self-assembly process appears to be dynamic, which is a sharp contrast to our previous static INCP examples.[11]

These particular 2D sheets can be compared to previous report on lamella nanocrystals from polyethylene (PE) where their thickness did not depend on the molecular weight of PE,[22] whereas the height of 2D nanosheets here was directly proportional to $M_n$ of **P3**. The main difference may be the rigidity of the polymer backbone. PE is most well-known for its crystalline lamella formation via extensive chain-folding. However, since **P3** with exclusive *trans* configuration is quite rigid and stretched, chain-folding is unlikely, and this is why one observes a unique strong linearity between the $M_n$ and the height of the 2D nanosheets.

Since semiconducting **P3** was also a fluorescent polymer (Figure S17),[23] we could directly visualize these well-ordered microsized 2D rectangles by laser scanning confocal microscopy (LSCM), revealing a large population of rectangles using various excitation wavelengths (488, 543, 592, and 633 nm) without the introduction of a fluorescent dye (Figures 6a and S18−S20). Furthermore, magnified images from super-resolution structured illumination microscopy (SR-SIM) showed a clear rectangular geometry (Figure 6b). Some images appeared to be hollow especially for SR-SIM images (Figure 6b) presumably due to fluorescence quenching from the area of the stacked rectangles. In addition to the dry film state, we could take a video of the fluorescent 2D rectangles of $\mathbf{P3}_{22}$ in chloroform solution by LSCM and watch in real time the free migration, rotation, and even collision of the 2D rectangles, while maintaining their shape and fluorescence (Figure 6c and Video S1). This confirmed that $\mathbf{P3}_{22}$ formed the resulting 2D rectangles in solution and that their nanostructures and photophysical property were sufficiently stable.

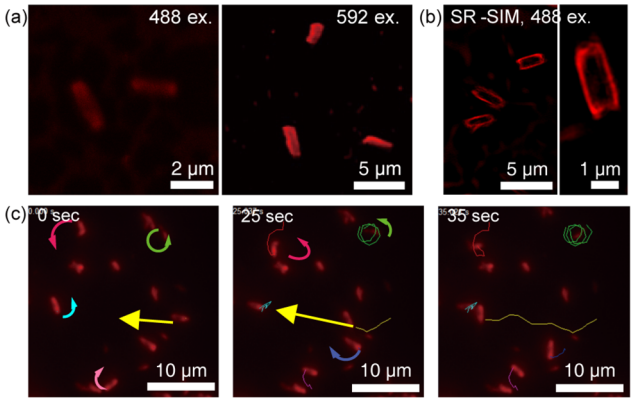


**Figure 6.** (a) LSCM images of 2D rectangles using an excitation wavelength ($\lambda_{ex}$) of 488 and 592 nm (spin-coating, 1 mg/mL) (b) SR-SIM image of 2D rectangles with 488 nm excitation. (c) Images captured at 0, 25, and 35 s from Video S1 showing the dynamics of 2D rectangles in chloroform solution (0.1 mg/mL, video rate = 20 fps).

## CONCLUSION

In summary, we demonstrated a simple *in situ* synthesis of 2D nanosheets by the living cyclopolymerization of a 1,6-heptadiyne monomer containing a fluorene moiety with neohexyl side chains. In all three solvents, 1 mg/mL solution of $\mathbf{P3}_{22}$ formed the most uniform 2D sheets. The DP of **P3** determined the average height of these 2D sheets. Based on the diffraction patterns of these 2D sheets obtained from FXRD and HR-TEM analyses, we proposed a unique slip-stack packing model with an intercalating 2D arrangement of **P3** showing interdigitation between the fluorene rings and neohexyl side chains. Furthermore, a new orthorhombic crystalline lattice accounted for the formation of highly ordered crystalline 2D rectangles from the most extended conformation of **P3** in chloroform as well as the absence of conventional $\pi-\pi$ interactions, which were generally observed from typical semicrystalline conjugated polymers. These 2D nanosheets were fluorescent enough for optical and super-resolution imaging, thereby revealing the real-time dynamics of the individual nanostructures in solution. We are currently studying the detailed INCP process to understand the solvent dependences of these different 2D shapes and how the chemical structures of the analogous polymers affected their self-assemblies.

## ASSOCIATED CONTENT

### Supporting Information

The Supporting Information is available free of charge on the ACS Publications website at DOI: 10.1021/jacs.6b12378.

Experimental details and further characterization data, including Figures S1−S20 and Tables S1 and S2 (PDF)
Video S1, showing the fluorescent 2D rectangles (AVI)
X-ray crystallographic data for **M3** (CIF)

## AUTHOR INFORMATION

### Corresponding Author

*tlc@snu.ac.kr

### ORCID

Sanghee Yang: 0000-0001-7944-6635
Tae-Lim Choi: 0000-0001-9521-6450

### Notes

The authors declare no competing financial interest.

## ACKNOWLEDGMENTS

This manuscript is dedicated to Prof. Bob Grubbs on the occasion of his 75th birthday. We are grateful to Prof. Wanchul Shin at SNU for his insightful help on the X-ray analysis. S.Y.



DOI: 10.1021/jacs.6b12378
J. Am. Chem. Soc. 2017, 139, 3082−3088

was supported by a National Research Foundation of Korea grant funded by the Korean government (NRF Fostering Core Leaders of the Future Basic Science Program/Global Ph.D. Fellowship Program, grant no. NRF-2015H1A2A1033703). Financial support from the Basic Science Research Program and the Nano-Material Technology Development Program through the NRF of Korea is acknowledged. We thank NICEM at SNU for supporting FXRD and LSCM, NCIRF at SNU for supporting SR-SIM, and LINC at Sogang University for supporting HR-MS experiments.

## REFERENCES

(1) Mai, Y.; Eisenberg, A. *Chem. Soc. Rev.* **2012**, *41*, 5969−5985.
(2) Zhang, L.; Eisenberg, A. *Science* **1995**, *268*, 1728−1731.
(3) (a) Kinning, D. J.; Winey, K. I.; Thomas, E. L. *Macromolecules* **1988**, *21*, 3502−3506. (b) Cui, H.; Chen, Z.; Zhong, S.; Wooley, K. L.; Pochan, D. J. *Science* **2007**, *317*, 647−650. (c) Rupar, P. A.; Chabanne, L.; Winnik, M. A.; Manners, I. *Science* **2012**, *337*, 559−562. (d) Li, Z.; Ma, J.; Lee, N. S.; Wooley, K. *J. Am. Chem. Soc.* **2011**, *133*, 1228−1231. (e) Gröschel, A. H.; Schacher, F. H.; Schmalz, H.; Borisov, O. V.; Zhulina, E. B.; Walther, A.; Müller, A. H. E. *Nat. Commun.* **2012**, *3*, 710.
(4) Pecher, J.; Mecking, S. *Chem. Rev.* **2010**, *110*, 6260−6279.
(5) (a) Grimsdale, A. C.; Chan, K. L.; Martin, R. E.; Jokisz, P. G.; Holmes, A. B. *Chem. Rev.* **2009**, *109*, 897−1092. (b) Wu, C.; Szymanski, C.; Cain, Z.; McNeill, J. *J. Am. Chem. Soc.* **2007**, *129*, 12904−12905.
(6) (a) Liu, J.; Sheina, E.; Kowalewski, T.; McCullough, R. D. *Angew. Chem., Int. Ed.* **2002**, *41*, 329−332. (b) Ho, V.; Boudouris, B. W.; McCulloch, B. L.; Shuttle, C. G.; Burkhardt, M.; Chabinyc, M. L.; Segalman, R. A. *J. Am. Chem. Soc.* **2011**, *133*, 9270−9273. (c) Patel, S. N.; Javier, A. E.; Balsara, N. P. *ACS Nano* **2013**, *7*, 6056−6068.
(7) Liu, C.; Wang, K.; Gong, X.; Heeger, A. J. *Chem. Soc. Rev.* **2016**, *45*, 4825−4846.
(8) (a) Kamps, A. C.; Cativo, M. H. M.; Fryd, M.; Park, S.-J. *Macromolecules* **2014**, *47*, 161−164. (b) Cambridge, G.; Gonzalez-Alvarez, M. J.; Guerin, G.; Manners, I.; Winnik, M. A. *Macromolecules* **2015**, *48*, 707−716.
(9) Huang, Y.; Mai, Y.; Yang, X.; Beser, U.; Liu, J.; Zhang, F.; Yan, D.; Müllen, K.; Feng, X. *J. Am. Chem. Soc.* **2015**, *137*, 11602−11605.
(10) Patra, S. K.; Ahmed, R.; Whittell, G. R.; Lunn, D. J.; Dunphy, E. L.; Winnik, M. A.; Manners, I. *J. Am. Chem. Soc.* **2011**, *133*, 8842−8845.
(11) (a) Yoon, K.-Y.; Lee, I.-H.; Kim, K. O.; Jang, J.; Lee, E.; Choi, T.-L. *J. Am. Chem. Soc.* **2012**, *134*, 14291−14294. (b) Lee, I.-H.; Amaladass, P.; Choi, T.-L. *Chem. Commun.* **2014**, *50*, 7945−7948. (c) Lee, I.-H.; Amaladass, P.; Yoon, K.-Y.; Shin, S.; Kim, Y.-J.; Kim, I.; Lee, E.; Choi, T.-L. *J. Am. Chem. Soc.* **2013**, *135*, 17695−17698. (d) Shin, S.; Yoon, K.-Y.; Choi, T.-L. *Macromolecules* **2015**, *48*, 1390−1397.
(12) (a) Li, Y.; Armes, S. P. *Angew. Chem., Int. Ed.* **2010**, *49*, 4042−4046. (b) Blanazs, A.; Madsen, J.; Battaglia, G.; Ryan, A. J.; Armes, S. P. *J. Am. Chem. Soc.* **2011**, *133*, 16581−16587. (c) Sugihara, S.; Blanazs, A.; Armes, S. P.; Ryan, A. J.; Lewis, A. L. *J. Am. Chem. Soc.* **2011**, *133*, 15707−15713.
(13) (a) Schwierz, F. *Nat. Nanotechnol.* **2010**, *5*, 487−496. (b) Chen, L.; Hernandez, Y.; Feng, X.; Müllen, K. *Angew. Chem., Int. Ed.* **2012**, *51*, 7640−7654.
(14) (a) Boott, C. E.; Nazemi, A.; Manners, I. *Angew. Chem., Int. Ed.* **2015**, *54*, 13876−13894. (b) Kissel, P.; Erni, R.; Schweizer, W. B.; Rossell, M. D.; King, B. T.; Bauer, T.; Götzinger, S.; Schlüter, A. D.; Sakamoto, J. *Nat. Chem.* **2012**, *4*, 287−291. (c) Kory, J. M.; Wörle, M.; Weber, T.; Payamyar, P.; van de Poll, S. W.; Dshemuchadse, J.; Trapp, N.; Schlüter, A.D. *Nat. Chem.* **2014**, *6*, 779−784. (d) Baek, K.; Yun, G.; Kim, Y.; Kim, D.; Hota, R.; Hwang, I.; Xu, D.; Ko, Y. H.; Gu, G. H.; Suh, J. H.; Park, C. G.; Sung, B. J.; Kim, K. *J. Am. Chem. Soc.* **2013**, *135*, 6523−6528. (e) Baek, K.; Xu, D.; Murray, J.; Kim, S.; Kim, K. *Chem. Commun.* **2016**, *52*, 9676−9678.
(15) Cativo, M. H. M.; Kim, D. K.; Riggleman, R. A.; Yager, K. G.; Nonnenmann, S. S.; Chao, H.; Bonnell, D. A.; Black, C. T.; Kagan, C. R.; Park, S.-J. *ACS Nano* **2014**, *8*, 12755−12762.
(16) (a) Hudson, Z. M.; Boott, C. E.; Robinson, M. E.; Rupar, P. A.; Winnik, M. A.; Manners, I. *Nat. Chem.* **2014**, *6*, 893−898. (b) Qiu, H.; Gao, Y.; Boott, C. E.; Gould, O. E. C.; Harniman, R. L.; Miles, M. J.; Webb, S. E. D.; Winnik, M. A.; Manners, I. *Science* **2016**, *352*, 697−701. (c) Rizis, G.; van de Ven, T. G. M.; Eisenberg, A. *Angew. Chem., Int. Ed.* **2014**, *53*, 9000−9003. (d) Rizis, G.; van de Ven, T. G. M.; Eisenberg, A. *ACS Nano* **2015**, *9*, 3627−3640.
(17) (a) Fox, H. H.; Wolf, M. O.; O'Dell, R.; Lin, B. L.; Schrock, R. R.; Wrighton, M. S. *J. Am. Chem. Soc.* **1994**, *116*, 2827−2843. (b) Anders, U.; Nuyken, O.; Buchmeiser, M. R.; Wurst, K. *Angew. Chem., Int. Ed.* **2002**, *41*, 4044−4047. (c) Krause, J. O.; Zarka, M. T.; Anders, U.; Weberskirch, R.; Nuyken, O.; Buchmeiser, M. R. *Angew. Chem., Int. Ed.* **2003**, *42*, 5965−5969. (d) Kumar, P. S.; Wurst, K.; Buchmeiser, M. R. *J. Am. Chem. Soc.* **2009**, *131*, 387−395. (e) Kang, E.-H.; Lee, I. S.; Choi, T.-L. *J. Am. Chem. Soc.* **2011**, *133*, 11904−11907. (f) Kim, J.; Kang, E.-H.; Choi, T.-L. *ACS Macro Lett.* **2012**, *1*, 1090−1093.
(18) Fleming, S.; Ulijn, R. V. *Chem. Soc. Rev.* **2014**, *43*, 8150−8177.
(19) Kang, E.-H.; Choi, T.-L. *ACS Macro Lett.* **2013**, *2*, 780−784.
(20) (a) Prosa, T. J.; Winokur, M. J.; Moulton, J.; Smith, P.; Heeger, A. J. *Macromolecules* **1992**, *25*, 4364−4372. (b) Colle, R.; Grosso, G.; Ronzani, A.; Zicovich-Wilson, C. M. *Phys. Status Solidi B* **2011**, *248*, 1360−1368. (c) Dong, H.; Jiang, S.; Jiang, L.; Liu, Y.; Li, H.; Hu, W.; Wang, E.; Yan, S.; Wei, Z.; Xu, W.; Gong, X. *J. Am. Chem. Soc.* **2009**, *131*, 17315−17320.
(21) Bhayana, B.; Wilcox, C. S. *Angew. Chem., Int. Ed.* **2007**, *46*, 6833−6836.
(22) (a) Weber, C. H. M.; Chiche, A.; Krausch, G.; Rosenfeldt, S.; Ballauff, M.; Harnau, L.; Göttker-Schnetmann, I.; Tong, Q.; Mecking, S. *Nano Lett.* **2007**, *7*, 2024−2029. (b) Osichow, A.; Rabe, C.; Vogtt, K.; Narayanan, T.; Harnau, L.; Drechsler, M.; Ballauff, M.; Mecking, S. *J. Am. Chem. Soc.* **2013**, *135*, 11645−11650.
(23) McQuade, D. T.; Kim, J.; Swager, T. M. *J. Am. Chem. Soc.* **2000**, *122*, 5885−5886.


DOI: 10.1021/jacs.6b12378
*J. Am. Chem. Soc.* 2017, 139, 3082−3088